High-Resolution Soft X-Ray Spectral Analysis in the C*K* Region of Titanium Carbide (TiC) using the DV-Xα Molecular Orbital Method

Kenta Shimomura[1], Yasuji Muramatsu[1], Jonathan D. Denlinger[2], and Eric M. Gullikson[2]

[1] *Graduate School of Engineering, University of Hyogo, 2167 Shosha, Himeji, Hyogo 671-2201, Japan*

[2] *Lawrence Berkeley National Laboratory, 1 Cyclotron Road, Berkeley, CA 94720, USA*

Keyword

titanium carbide, soft X-ray spectroscopy, electronic structure, chemical analysis, DV-Xα

Abstract

We used the DV-Xα method to analyze the high-resolution soft X-ray emission and absorption spectra in the C*K* region of titanium carbide (TiC). The spectral profiles of the X-ray emission and absorption can be successfully reproduced by the occupied and unoccupied density of states (DOS), respectively, in the C2p orbitals of the center carbon atoms in a $Ti_{62}C_{63}$ cluster model, suggesting that the center carbon atom in a large cluster model expanded to the cubic-structured 5^3 (= 125) atoms provides sufficient DOS for the X-ray spectral analysis of rock-salt structured metal carbides.

Introduction

Soft X-ray emission and X-ray absorption spectroscopy using synchrotron radiation (SR) has recently become a powerful tool for electronic-structure and chemical-state analyses of industrial carbon materials [1]. Compared to other spectroscopic methods, this spectroscopy has remarkable advantages. The first is high-resolution measurements, which enable finer information about the electronic structure and chemical states to be obtained. The second is orbital or site selectivity due to the selection rule of the dipole transition, and the third is band-gap analysis by combining X-ray emission and absorption spectroscopy. From a spectral analysis viewpoint, it is well known that the discrete variational (DV) –X α molecular orbital method [2] is a powerful tool for theoretical analysis of the X-ray emission [3] and X-ray absorption [4, 5] spectroscopy, especially for carbon materials [6]. However, carbon in metals, such as metal carbides and carbon/metal alloys, is generally a difficult target for spectral measurements by soft X-ray emission and absorption spectroscopy due to the lower X-ray fluorescence yield of carbon compared to that of the metal, as well as for theoretical spectral analysis due to the complicated orbital hybridizations between the C2s/C2p orbitals and the metal valence s/p/d/f orbitals.

Various metal/carbon systems, for example MC (M: Zr, Hf, V, Nb, Ta) [7], TiC [7-9], SiC [10], Ti_4SiC_3 [11], and UC [12], have been analyzed by combining soft X-ray spectroscopy and/or the DV-Xα method. However, the previously reported X-ray spectral profiles occasionally appear to have a lower resolution, and the spectral simulations using the DV-Xα method often seem to be insufficient for the high-resolution spectral profiles. Thus, to demonstrate the powerfulness of the DV-Xα method, we measured high-resolution soft X-ray emission and absorption spectra in the C*K* region of metal carbides, and analyzed the spectral profiles using the DV-Xα method with a sufficiently large cluster models. Herein we focused on titanium carbide (TiC) due to its simple rock-salt structure.

High-resolution soft X-ray emission and absorption spectra

The samples were commercially available TiC powder (Nilaco Co., purity > 98%, average particle size = 1.8 μm) and highly oriented pyrolytic graphite (HOPG), which served as a reference. Figure 1, which shows the X-ray diffraction (XRD) pattern of the TiC sample, confirms that TiC has a rock-salt structure with negligible impurities. High-resolution soft X-ray emission and absorption spectral measurements in the C *K* region were performed in beamline BL-8.0.1 [13] and BL-6.3.2 [14], respectively, at the Advanced Light Source (ALS). In the X-ray emission spectra (XES) measurements, the undulator beams, which were monochromatized at 320 eV, were incident to the TiC sample, and the emitted C*K* fluorescent X-rays were monochromatized by a Rowland-mount grating spectrometer with an estimated energy resolution (E/ΔE) of 2000. In the X-ray absorption spectra (XAS) measurements, the photocurrent of the sample was monitored while scanning of the incident monochromatized SR beam, which provided the total-electron-yield (TEY) XAS. The estimated energy resolution of the XAS measurements with a variable-line-spacing grating (average groove density = 600 mm^{-1}) and 40-μm slits was 4000. Details of the XES and XAS measurements can be found elsewhere [1].

Figure 2 shows the measured XES and XAS in the C *K* region of TiC and the reference HOPG. In the XES, TiC was represented by a main peak (denoted by *b*) at 279 eV with a low-energy small peak (*a*) at 277.5 eV and a high-energy shoulder (*c*) around 281 eV. This spectral profile agrees with previously published data [9, 15]. The spectral width of TiC (approximately 6 eV in full width) was narrower than that of HOPG (>15 eV), implying that the carbon atoms in TiC have an ionic character, while those in HOPG have a covalent character. In the XAS of TiC, two sharp peaks (*e*, *f*) were observed at 285 eV and 285.5 eV, and a shoulder (*d*) was observed at the threshold around 282 eV. These two peaks with a

threshold shoulder are characteristic of the C*K*-XAS of TiC.

Spectral analysis by the DV-Xα calculations

To analyze the spectral fine structures in the C *K* XES and XAS of TiC, the occupied and unoccupied density of states (DOS) of various Ti_xC_y cluster models were calculated using commercially available DV-Xα software. As shown in Fig. 3, the Ti_xC_y cluster models were Ti_6C_7, $Ti_{19}C_6$, $Ti_{14}C_{19}$, and $Ti_{62}C_{63}$. In the smallest Ti_6C_7 model, the center C atom was surrounded by six 1st-neighbor Ti atoms and six 2nd-neighbor C atoms. In the $Ti_{19}C_6$ model, which is the model previously calculated by Song [9], the center Ti atom was surrounded by six 1st-neighbor C atoms and eighteen 2nd-neighbor Ti atoms. In the $Ti_{14}C_{19}$ model, the center C atom was surrounded by six 1st-neighbor Ti atoms and eighteen 2nd-neighbor C atoms. The largest $Ti_{62}C_{63}$ model was expanded from $Ti_{14}C_{19}$ to shape a cubic structure composed of 5 x 5 x 5 (= 125) atoms. The Ti-C bond length in the cluster models was set at 2.1645 Å, which corresponds to the typical lattice parameter of a TiC crystal. The DV-Xα calculations were performed in the ground-states with a basis set of 1s, 2s, and 2p orbitals for C atoms, and 1s, 2s, 2p, 3s, 3p, 3d, 4s, and 4p orbitals for Ti atoms. The calculated DOS of the target atoms in the cluster models were broadened with a 0.5-eV wide Lorentzian functions in order to compare to the measured XES and XAS profiles. The molecular orbital (MO) energy was corrected at the highest occupied molecular orbital (HOMO) as 0 eV.

Figure 4 compares the occupied C2s- and C2p-DOS of the center C atom in the Ti_6C_7, $Ti_{14}C_{19}$, and $Ti_{62}C_{63}$ models as well as the 1st-neighbor C atom in the $Ti_{19}C_6$ model to the C*K*-XES. According to the selection rule for dipole transitions, the C *K* XES should be compared to C2p-DOS. The smallest Ti_6C_7 model, which was represented by a single peak in the C2p-DOS, could not reproduce the XES profile. The $Ti_{19}C_6$ and $Ti_{14}C_{19}$ models were represented by broader C2p-DOS with three peak components. Similar to the smallest model,

the peak intensity ratio among the components could not reproduce the XES profile. On the other hand, the C2p-DOS of the $Ti_{62}C_{63}$ reproduced the XES features by the low-energy small peak (*a*), the main peak (*b*), and the high-energy shoulder (*c*).

Similar results were obtained by comparing the unoccupied C2p-DOS to the measured C*K*-XAS, as shown in Fig. 5. The unoccupied C2p-DOS in the 0 – 10 eV region of the Ti_6C_7, $Ti_{19}C_6$, and $Ti_{14}C_{19}$ models represented a multi-peak structure. However, their peak intensity ratio and the energy-span among the peaks could not reproduce the XAS profile. On the other hand, the C2p-DOS of the $Ti_{62}C_{63}$ model was represented by three peaks with an intensity ratio and energy span that exactly reproduced the threshold shoulder (*d*) and the two peaks (*e*, *f*) in the XAS. Thus, it is confirmed that the $Ti_{62}C_{63}$ model has a sufficient cluster size and shape for spectral analysis of the C *K*-XES and XAS of TiC using the DV-Xα method.

Figure 6 compares the occupied DOS of the center C atom and the 1st-neighbor Ti atom in the $Ti_{62}C_{63}$ model with the C *K*-XES and previously reported photoelectron spectrum (PS) [16]. However, DOS of the Ti3s and Ti3p orbitals are not described in the figure because their MO energy is deeper than -20 eV and their hybridizations with C2p orbital is negligible. The main peak (*b*) in the XES was attributed to the hybridization of C 2p with the Ti3d and Ti4d orbitals, while the low-energy peak (*a*) was due to the C2p with Ti3d, Ti4s, and Ti4p orbitals, and the high-energy shoulder (*c*) was attributed to the C2p with Ti3d and Ti4p orbitals. The total DOS of the C and Ti atoms, which was represented two peaks around -3 eV and -12 eV in MO energy, well reproduced the two-peak feature of the XPS. Especially, the lower-energy peak in the XPS was attributed mainly to the deeper C2s with Ti4s and Ti4p orbitals. Hence, it is confirmed that the fine structure of the C*K*-XES can be explained by the hybridization of the valence orbitals between C and Ti atoms. Figure 7 compares the unoccupied DOS of the center C atom and the 1st-neighbor Ti atom to the C*K*-XAS, but the

unoccupied DOS of the Ti3s and Ti3p orbitals are not described. Threshold shoulder (*d*) at the threshold in the XAS is attributed to the hybridization of C2p with Ti3d and Ti4s orbitals. Peak (*e*) was attributed to the C2p with a slight influence of C2s, Ti3d, and Ti4s orbitals. Peak (*f*) was due to the C2p with C2s and Ti3d orbitals. Therefore, it is confirmed that the fine structure at the C *K* absorption edge in the XAS of TiC can be well explained by the hybridization of the unoccupied orbitals of C and Ti atoms.

Conclusion

To analyze the high-resolution XES and XAS in the C*K* region of TiC using the DV-Xα method, DOS of various Ti_xC_y cluster models were calculated and compared to the C*K*-XES and XAS profiles. The occupied and unoccupied C2p-DOS of the center C atom in the $Ti_{62}C_{63}$ model successfully reproduced the XES and XAS profiles, respectively. From the DOS distribution of the valence and conduction orbitals in the center C and the 1st-neighbor Ti atom, the spectral fine structure of XES and XAS could be understood by the hybridization between them. These observations indicate that a cluster model composed of cubic-structured 5^3 (=125) atoms is necessary in DV-Xα calculations to exactly reproduce the XES and XAS profiles of rock-salt type metal carbide, and that the DV-Xα method can achieve reliable XES/XAS spectral analysis for carbon in metal matrices.

Acknowledgments

The authors would like to thank Professor Masataka Mizuno of Osaka University for his helpful discussions on the DV-Xα calculations. This work was supported by a Grant-in-Aid from the Ministry of Education, Culture, Sports, Science and Technology of Japan under contract No. 20560628, and by the U.S. Department of Energy at the ALS under contract No. DE-AC02-05CH11231.

References

1. Muramatsu, Y. ; Hayashi, T., Adv. X-Ray Chem. Anal. Jpn. 1999, 30, 41-53.

2. Adachi, H.; Tsukada, M.; Satoko, C., J. Phys. Soc. Jpn., 1978, 45, 875-883.

3. Taniguchi, K.; Adachi, H., J. Phys. Soc. Jpn., 1980, 49, 1944.

4. Nakamatsu, H.; Mukoyama, T.; Adachi, H., J. Chem. Phys., 1991, 95, 3167.

5. Nakamatsu, H., Chem. Phys., 1995, 200, 49.

6. Muramatsu, Y.; Gullikson, E. M.; Perera, R. C. C., Adv. X-Ray Chem. Anal. Jpn., 2004, 35, 125-136.

7. Sekine, R.; Miyazaki, E.; Nakam atsu, H., Annu. Rep. DV-Xα Conference, 1994, 7(2), 253-257.

8. Sekine, R.; Nakamatsu, H.; Mukoyama, T.; Onoe, J.; Hirata, M.; Kurihara, M.; A dachi, H., Adv. Quantum Chem.,1998, 29, 123-136.

9. Song, B.; Naka matsu, H.; Sekine, R.; Mukoyama, T.; Taniguchi, K., J. Phys. Cond. Matt., 1998, 10, 9443–9454.

10. Muram atsu, Y.; Takenaka, H.; Ueno, Y .; Gulliks on, E. M.; Perera, R. C. C., Appl. Phys. Lett., 2000, 77, 2653-2655.

11. Magnuson, M.; Mattesini, M.; W ihelmsson, O. ; Emme rlich, J.; Palmquist, J. P .; Li, S.; Ahuja, R.; Hultman, L.; Eriksson, O.; Jansson, U., Phys. Rev. B, 2006, 74, 205102.

12. Kurihara, M.; Hirata, M.; Sekine, R.; Onoe, J.; Nakamatsu, H.; Mukoyama, T.; Adachi, H., J. Alloys Comp., 1999, 283, 128-132.

13. Jia, J. J.; Callcott, T. A.; Yurkas, J.; Ellis, A. W.; Himpsel, F. J.; Samant, M. G.; Stöhr, J.; Ederer, D. L.; Carlisle, J. A.; Hudson, E. A.; Terminello, L. J.; Shuh, D. K.; Perera, R. C C., Rev. Sci. Instrum., 1995, 66, 1394.

14. Underwood, J. H.; Gullikson, E . M.; Koike, M.; Batson, P . J.; Denham , P. E.; Franck, K. D.; Tackaberry, R. E.; Steele, W. F., Rev. Sci. Instrum., 1996, 67, 3372.

15. Magnuson, M., J. Phys. Conf. Series, 2007, 61, 760-764.

16. Johansson, L. I.; Stefan, P. M.; Shek, M. L.; Norlund Christensen, A., Phys. Rev. B, 1980, 22, 1032.

Figure Captions

Figure 1 XRD pattern of the measured TiC powder sample.

Figure 2 High-resolution X-ray emission (upper panel) and absorption (lower) spectra in the C*K* region of TiC and HOPG as a reference.

Figure 3 Ti_xC_y cluster models (Ti_6C_7, $Ti_{19}C_6$, $Ti_{14}C_{19}$, $Ti_{62}C_{63}$) for the DV-Xα calculations.

Figure 4 Occupied C2p and C2s-DOS of the Ti_xC_y cluster models compared to the C*K*-XES of TiC.

Figure 5 Unoccupied C2p and C2s-DOS of the Ti_xC_y cluster models compared to the C*K*-XAS of TiC.

Figure 6 Occupied DOS in the C2p, C2s, Ti3d, Ti4s, and Ti4p orbitals at the center C atom and the 1st-neighbor Ti atom in the $Ti_{62}C_{63}$ model compared to the C *K*-XES and the PS [16].

Figure 7 Unoccupied DOS in the C2p, C2s, Ti3d, Ti4s, and Ti4p orbitals at the center C atom and the 1st-neighbor Ti atom in the $Ti_{62}C_{63}$ model compared to the C*K*-XAS.

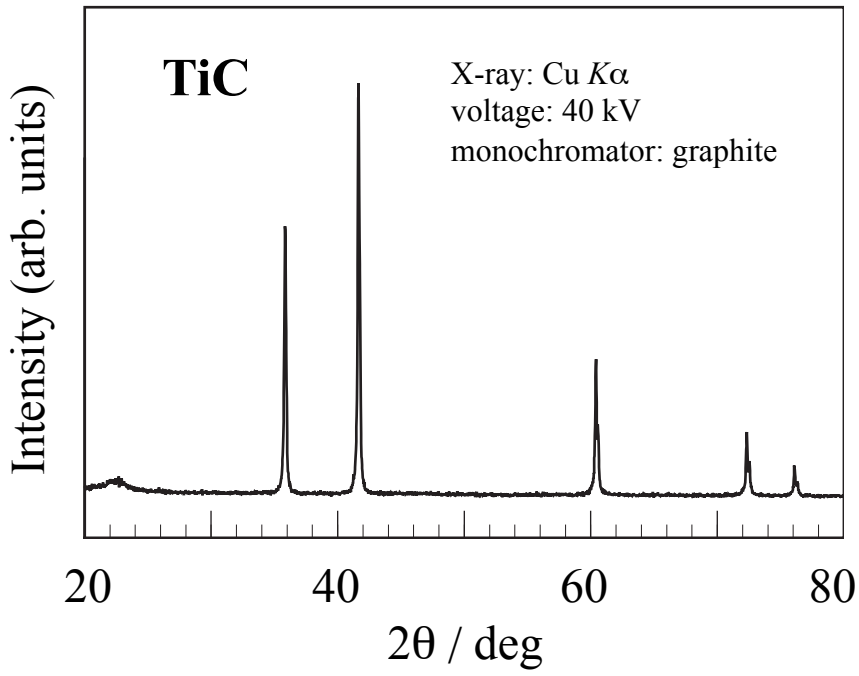

Figure 1 K. Shimomura

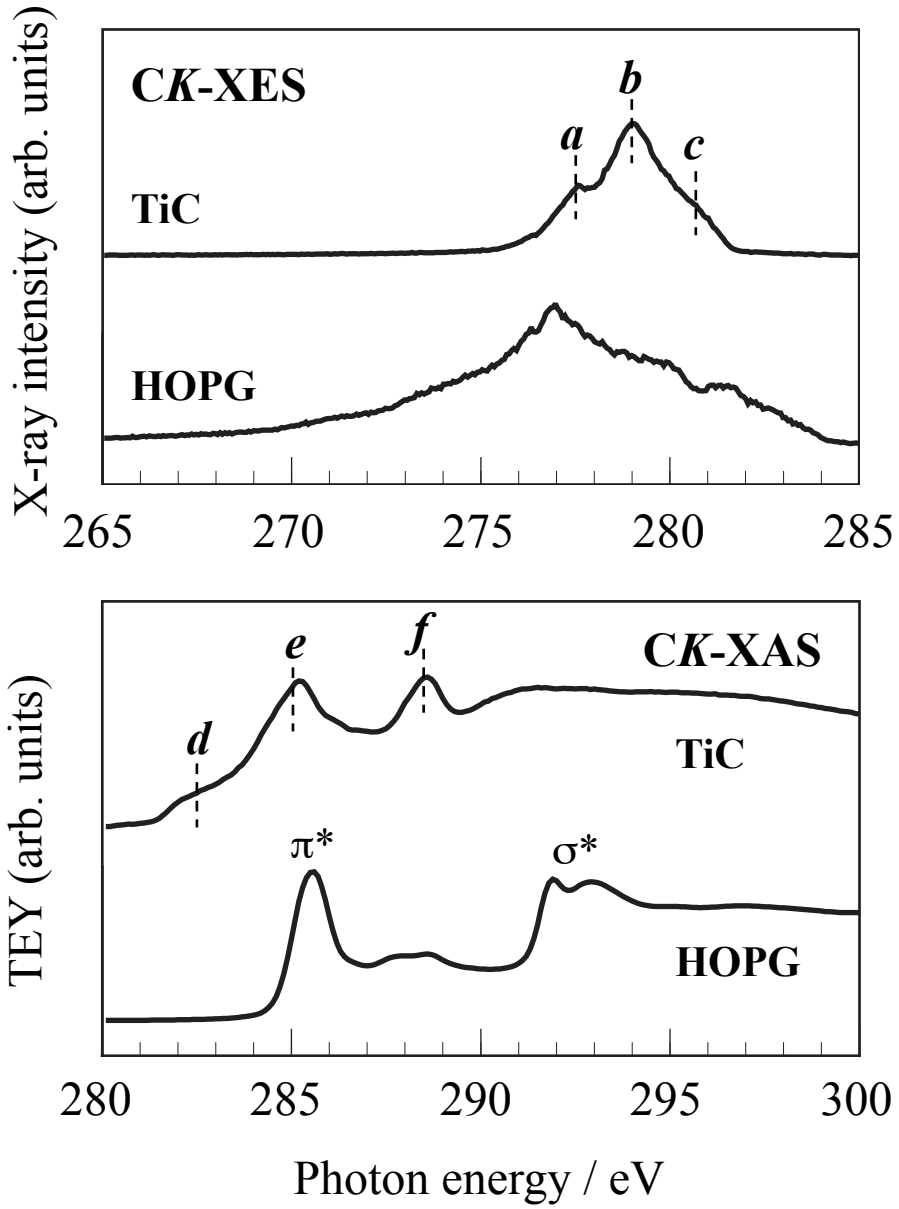

Figure 2 K. Shimomura

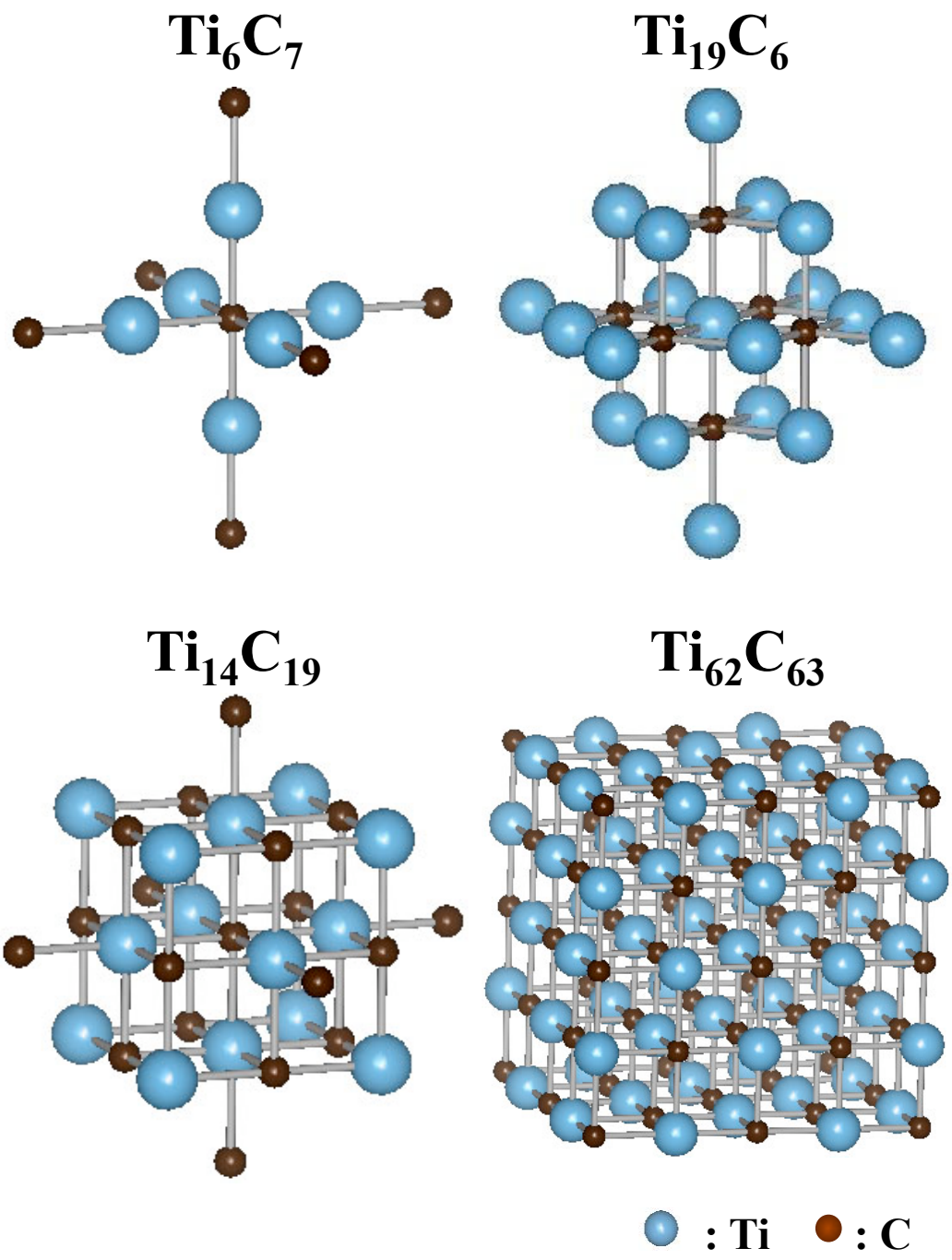

Figure 3 K. Shimomura

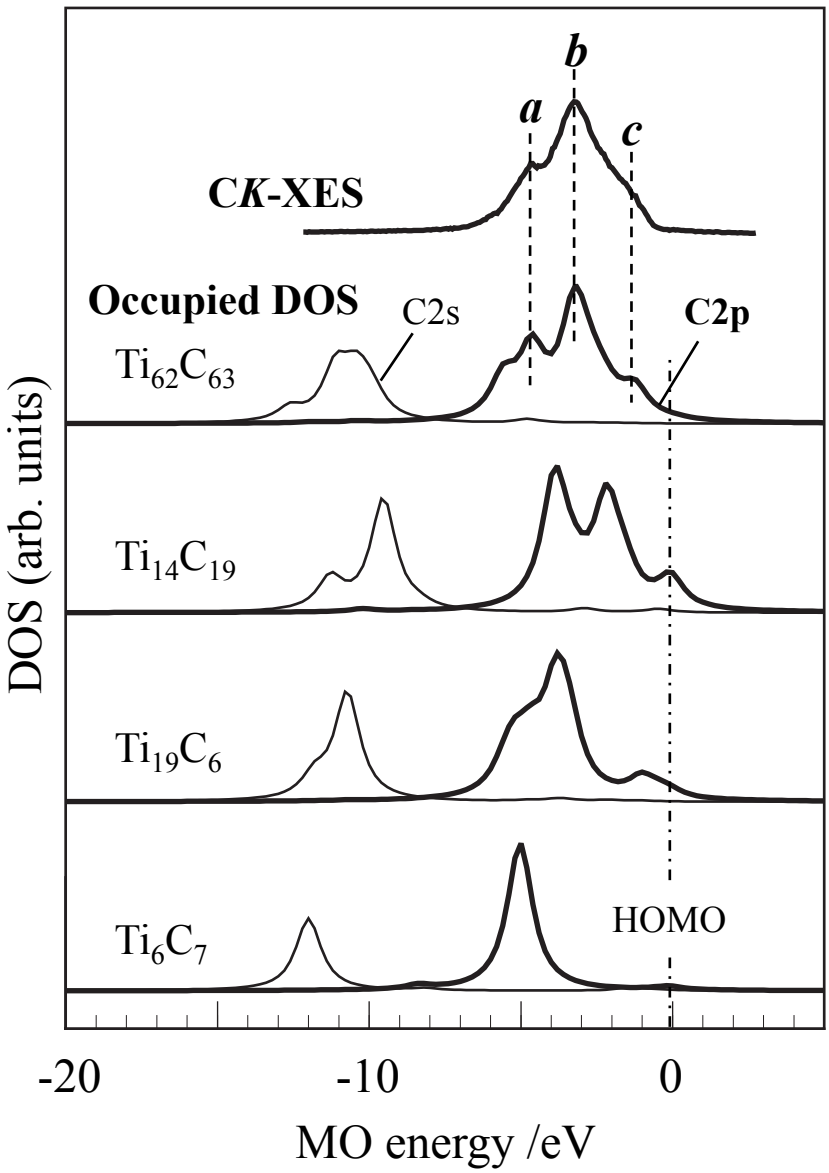

Figure 4 K. Shimomura

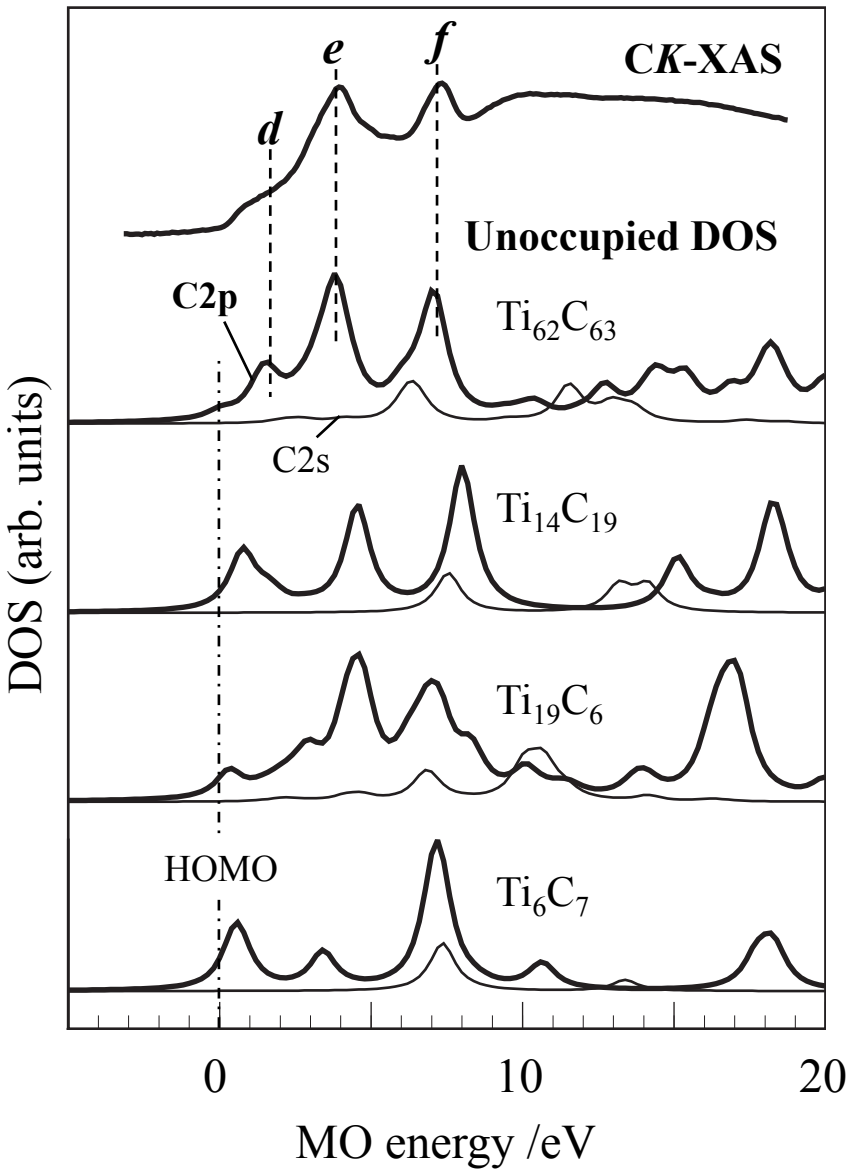

Figure 5 K. Shimomura

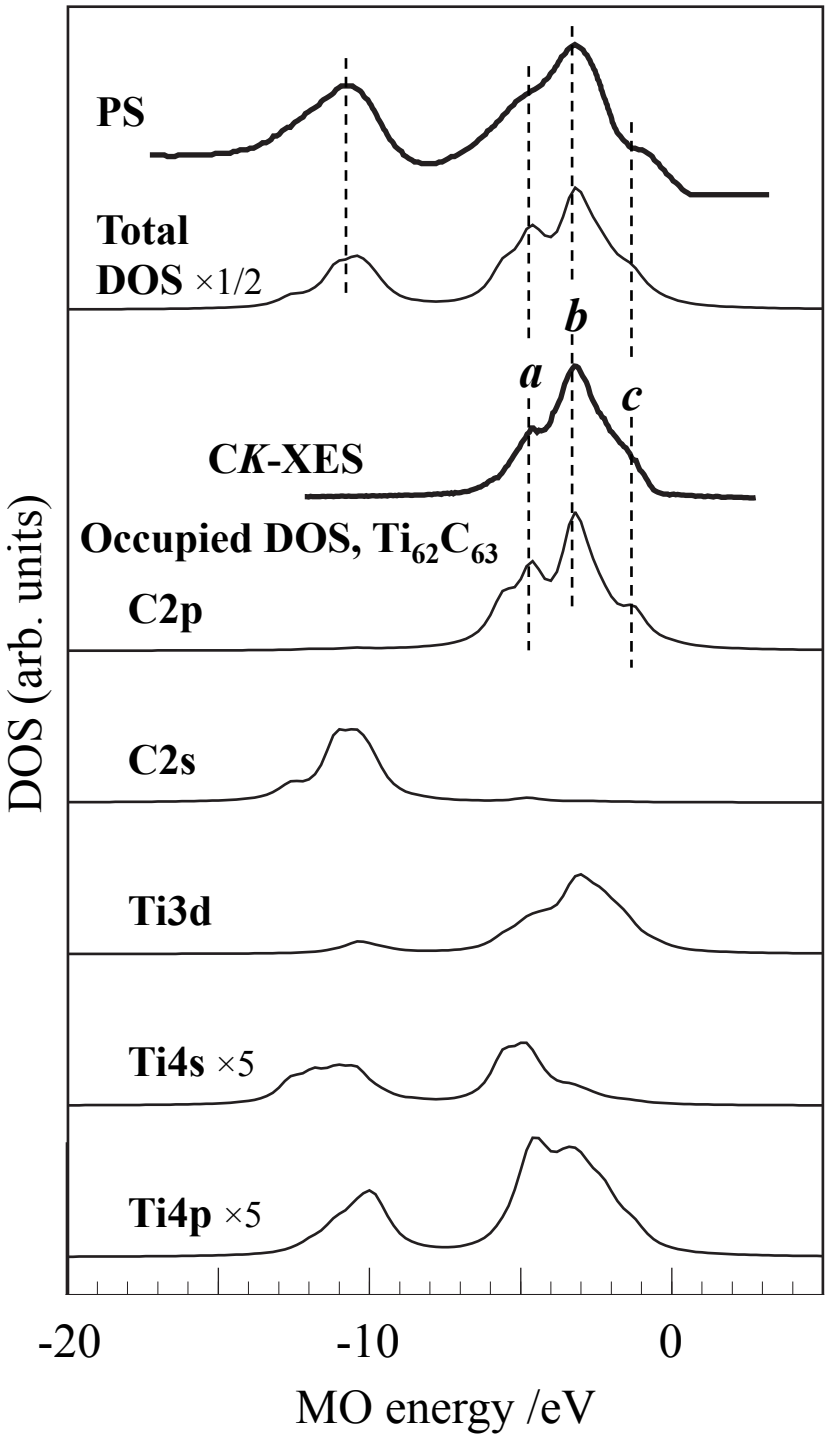

Figure 6 K. Shimomura

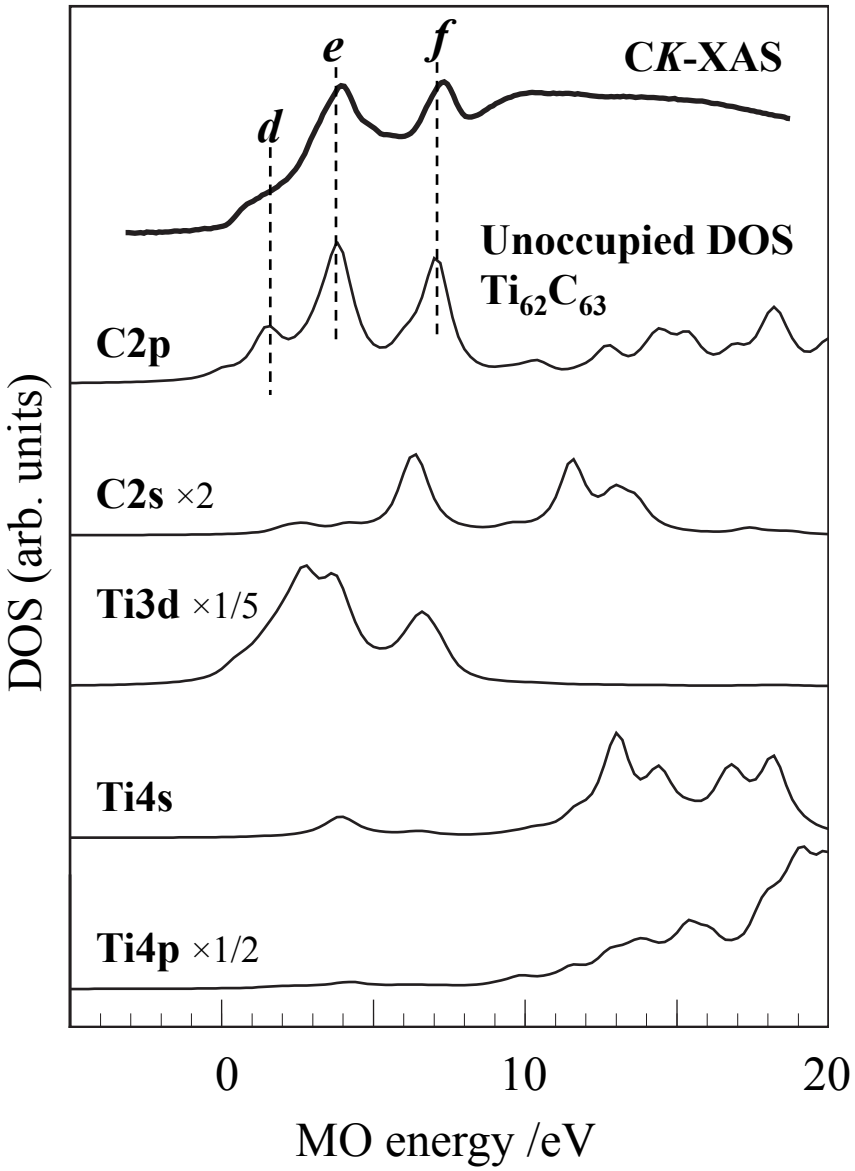

Figure 7 K. Shimomura